Available online at www.sciencedirect.com
SCIENCE DIRECT®
Surface Science 560 (2004) 235–245
SURFACE SCIENCE
www.elsevier.com/locate/susc

Adsorption and reaction of NO_2 on a $(\sqrt{3} \times \sqrt{3})R30°$ Sn/Pt(1 1 1) surface alloy

Michael R. Voss [1], Haibo Zhao, Bruce E. Koel *

Department of Chemistry, University of Southern California, SSC 606, Los Angeles, CA 90089-0482, USA

Received 21 November 2003; accepted for publication 16 March 2004
Available online 2 April 2004

Abstract

Adsorption of nitrogen dioxide (NO_2) on a $(\sqrt{3} \times \sqrt{3})R30°$ Sn/Pt(1 1 1) surface alloy has been investigated using temperature programmed desorption (TPD), Auger electron spectroscopy (AES), high-resolution electron energy loss spectroscopy (HREELS), and low energy electron diffraction (LEED). At 120 K, NO_2 is adsorbed molecularly as the *N*,*N*-bonded dimer, N_2O_4, interacting with the surface through a single oxygen atom in an upright but tilted geometry. However, no N_2O_4 or NO_2 desorbs molecularly from the monolayer state. The dimer completely dissociates at 300 K, leaving coadsorbed NO_2, NO, and O on the surface. Adsorbed NO_2 further dissociates to coadsorbed NO and O at 300–400 K. The maximum oxygen atom coverage obtained by heating the N_2O_4 monolayer was about $\theta_O = 0.4$ ML, but this can be increased to $\theta_O = 1.1$ ML by NO_2 dosing on the alloy surface at 600 K to remove inhibition by coadsorbed NO. Under these latter conditions, adsorbed oxygen desorbs as O_2 in three clear desorption states, the lowest of which is associated with O_2 desorption from Pt sites and the other two are from decomposition of reduced tin oxide phase(s), SnO_x. Shifts in Sn AES peaks were used to follow Sn oxidation.

Keywords: Nitrogen oxides; Chemisorption; Platinum; Tin; Alloys; Oxidation; Electron energy loss spectroscopy (EELS); Thermal desorption; Auger electron spectroscopy

1. Introduction

Nitrogen dioxide (NO_2) is a versatile ligand in inorganic chemistry, bonding to metal atoms in many distinct geometries [1]. Interactions of NO_2 with metal surfaces are important in many processes, e.g., automotive exhaust catalysis [2] and atmospheric NO_x measurement at very low concentrations [3]. A selective detector has also been developed that makes use of selective oxidation of organic compounds by NO_2 in the presence of gold or palladium catalysts [4]. Limited molecular-level information on the interaction of NO_2 with metal surfaces has inhibited understanding catalytic reaction mechanism involving nitrogen oxides. So far, adsorption and reaction of NO_2 has been investigated on Pt(1 1 1) [5,6], Ru(0 0 1) [7,8], Ag(1 1 0) [9,10], Ag(1 1 1) [11–13], Pd(1 1 1) [14], Au(1 1 1) [15–18].

* Corresponding author.
E-mail address: koel@usc.edu (B.E. Koel).
[1] Current address: Los Alamos National Laboratory, Los Alamos, NM 87545, USA.

0039-6028/$ - see front matter © 2004 Published by Elsevier B.V.
doi:10.1016/j.susc.2004.03.030

Previously, Bartram, et al. [5] used temperature programmed desorption (TPD) and high-resolution electron energy loss spectroscopy (HREELS) to study NO_2 adsorption on Pt(1 1 1). At 100 K, NO_2 is adsorbed molecularly at all coverages to form a Pt(1 1 1) μ-N,O-nitrito surface complex with C_s symmetry. The saturation coverage of chemisorbed NO_2 is about 0.5 monolayers (ML) at 100 K. At low coverages, $\theta_{NO_2} < 0.25$ ML, adsorption is irreversible and NO_2 dissociates completely by 285 K to O atoms and nitric oxide (NO). At larger NO_2 coverages, the adsorption is partially reversible and NO_2 desorbs molecularly with first-order kinetics and $E_a = 19$ kcal/mol. About 20% of the NO_2 desorbs reversibly at saturation coverage in the monolayer.

Platinum–tin bimetallic catalysts are of interest for selective oxidation and reduction reactions, and are commercially important for petroleum reforming [19]. Compared to Pt catalysts, Pt–Sn reforming catalysts have greater resistance to coking and increased selectivity to aromatics. Surface science model studies have addressed the effect of alloying Sn with Pt on hydrocarbon surface chemistry [20–26]. Industrial, supported, Pt–Sn catalysts, however, include an oxide support material and are complicated materials systems for which it is difficult to assess the phases present and the catalytic activity of each phase. It has been reported that on alumina, tin is partially oxidized [27] to create a mixed catalyst with a supported alloy phase PtSn/Al_2O_3 and a tin oxide-supported, Pt-phase Pt/SnO_x/Al_2O_3 [19], where the relative concentrations are determined mainly by particle size [28]. Specifically, the effect of tin oxidation on the kinetics of CO oxidation by O_2 on an α-Al_2O_3 supported, Pt–Sn catalyst has been studied by Grass and Lintz [29].

Of intense, additional interest, Pt-promoted SnO_2 thin films are used widely in sensor technologies, for example, in detection of ethanol [30] and CO [31]. These sensor systems are also complicated materials systems that could benefit greatly by surface science model studies that address the surface chemistry of Pt–Sn alloys and elucidate additional molecular-level information on the interaction of gases with these surfaces.

In this study, we investigate the chemistry of NO_2 on a $(\sqrt{3} \times \sqrt{3})R30°$ Sn/Pt(1 1 1) surface alloy. NO_2 is a reactive molecule, chemisorbing and dissociating on the alloy surface and eventually oxidizing the Sn from the alloy. Thus, NO_2 is a stronger oxidant than O_2 (O_2 does not dissociatively adsorb on Pt–Sn surface alloys under UHV conditions [32]) and is a useful precursor to produce surface oxygen species.

2. Experimental methods

Experiments were performed in a three-level UHV chamber as described earlier [33]. The Pt(1 1 1) crystal (Atomergic; 10 mm diameter, 1.5 mm thick) was prepared by 1-keV Ar^+-ion sputtering and oxygen treatment (5×10^{-7} Torr O_2, 900 K, 2 min) to give a clean spectrum using Auger electron spectroscopy (AES) and a sharp (1×1) pattern in low energy electron diffraction (LEED).

Sn was evaporated from a resistively heated, tantalum boat onto the sample, which was subsequently annealed to form a $(\sqrt{3} \times \sqrt{3})R30°$ Sn/Pt(1 1 1) surface alloy as described previously [34]. For convenience throughout this paper, we will refer to this surface as the "$\sqrt{3}$ alloy".

Nitrogen dioxide, NO_2, (Matheson, 99.5%) was used without additional purification. Portions of the gas handling line that remained under NO_2 pressure during dosing were passivated by baking in an NO_2 atmosphere for 1 h at 200 °C. Gold-plated Conflat® gaskets and stainless steel VCR® gaskets were used in the portion of the gas line in contact with NO_2 in order to minimize NO_2 decomposition. Still, the NO_2 line was pumped out and refilled after every dose to minimize NO_2 decomposition. NO_2 was leaked into the UHV chamber through a Varian® leak valve with an attached stainless steel tube and micro capillary array [35] to achieve a directed gas beam and exposure NO_2 on the sample without prior reaction with chamber walls. NO_2 exposures are reported using the background pressure measured indirectly by the ion gauge, ignoring doser enhancement effects and ion gauge sensitivity. NO_2 decomposes readily on the inner walls of the stainless steel dosing tube, and so the doser was passivated daily with an initial dose (60 s, 1×10^{-9} Torr) of NO_2. This was sufficient to maintain a

consistently high level of NO_2 purity for a single day's experiments, though it raised the background pressure of the chamber to 4×10^{-10} Torr. The NO_2 purity obtained by this method was characterized indirectly by a UTI 100C quadrupole mass spectrometer (QMS) monitoring the background gas in the chamber during dosing. The 30-amu (NO):46-amu (NO_2) ratio for the mass spectrometer signals during dosing was typically 50:1.

AES measurements were made with a double-pass cylindrical mirror analyzer (CMA). The electron gun was operated at 3-keV beam energy and 8-μA beam current. TPD experiments were done with a shielded QMS to reduce the electron flux on the sample. LEED patterns were recorded using four-grid optics and a CCD camera.

HREELS was performed by using an LK-2000 (LK Technologies) spectrometer system. HREELS spectra were recorded at a specular scattering angle of 30° from the surface plane with an average resolution of 55 cm^{-1} (6.8 meV) and a beam energy of 4.5 eV. The elastic peak for a clean surface had an intensity of 2×10^5 counts/s. We used a step size of about 5 cm^{-1} (0.6 meV) to record each spectrum and 10-point binomial smoothing routine to minimize noise. All of these spectra were recorded with the sample at 100 K, and inelastic losses are shown after normalization to elastic peak intensities.

Coverages θ_i reported in this paper are referenced to the surface atom density of Pt(1 1 1) such that $\theta_{Pt} = 1.0$ ML is defined as 1.505×10^{15} cm^{-2}. We will also use the terms monolayer and layer to refer to chemisorbed and physisorbed layers indicating whatever coverage is necessary to cover the surface.

3. Results

3.1. TPD

TPD spectra were obtained after exposures of NO_2 on the $\sqrt{3}$ Sn/Pt(1 1 1) surface alloy at 120 K. Fig. 1 shows NO_2 desorption traces obtained by monitoring the 46-amu signal. A single desorption peak appears below 150 K which increased in temperature with increasing coverage. This peak

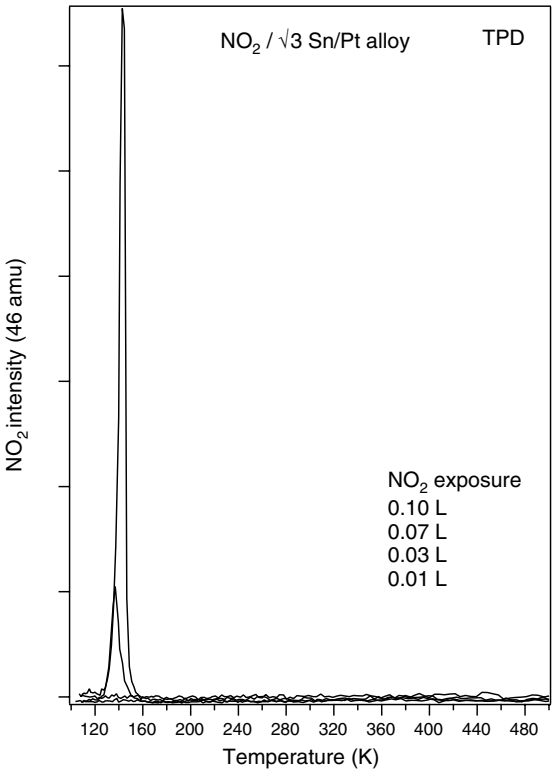

Fig. 1. NO_2 desorption spectra after NO_2 exposures on the $\sqrt{3}$ Sn/Pt(1 1 1) surface alloy at 120 K.

corresponds to desorption of NO_2 from multilayer, physisorbed species and occurs at the same temperature as that for Pt(1 1 1) [5]. However, unlike the case on Pt(1 1 1), no NO_2 desorbs from the chemisorbed monolayer. The NO_2 monolayer reacts completely and irreversibly on a $\sqrt{3}$ alloy surface. This can be compared to the decomposition of about 80% of the monolayer on Pt(1 1 1) [5].

Fig. 2 traces the evolution of one of the reaction products, NO, after increasing NO_2 exposures. The lowest exposure investigated yields three desorption peaks at 240, 280, and 360 K. After increasing NO_2 exposures, these NO desorption peaks saturate in size and shift to higher temperature. Desorption of NO under most of these conditions is reaction rate-limited, because NO desorption following NO adsorption on a $\sqrt{3}$ alloy occurs in a single peak which shifts with coverage from 240 to 190 K [36].

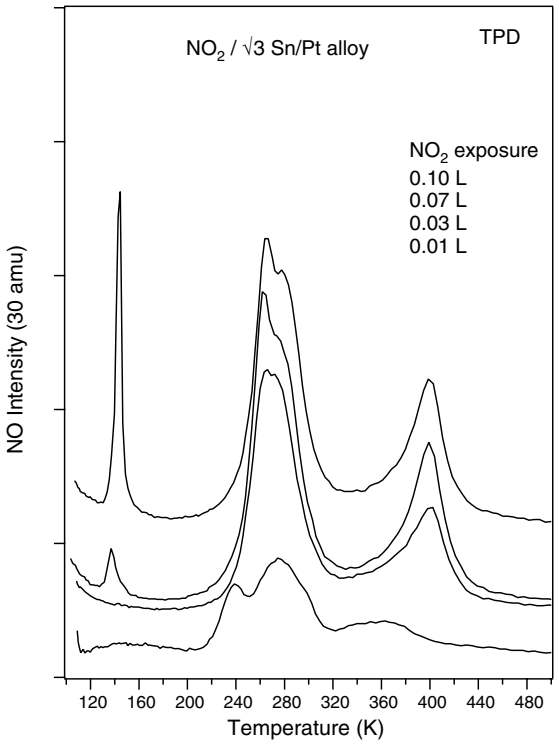

Fig. 2. NO desorption spectra resulting from NO_2 exposures to the $\sqrt{3}$ Sn/Pt(1 1 1) surface alloy at 120 K.

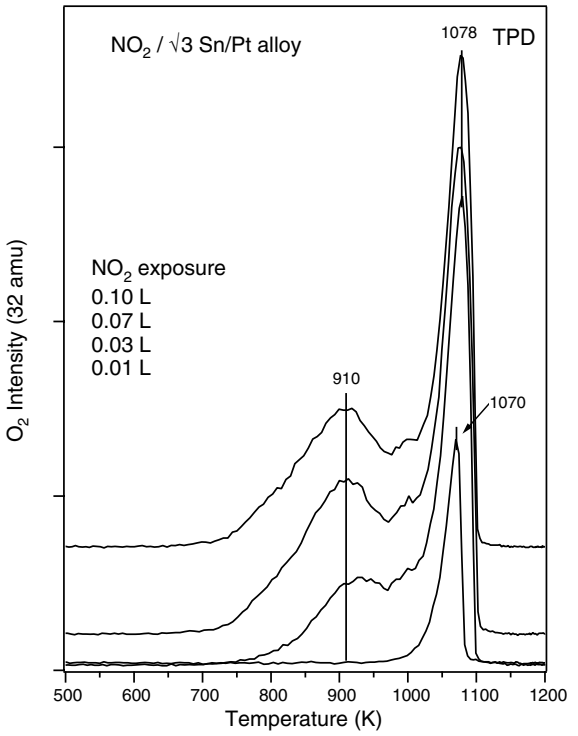

Fig. 3. O_2 desorption spectra resulting from NO_2 exposures to the $\sqrt{3}$ Sn/Pt(1 1 1) surface alloy at 120 K.

Fig. 3 shows corresponding O_2 TPD spectra obtained during the same experiments. After a small initial NO_2 dose, O_2 desorption occurred at 1070 K in a peak that shifts to 1077 K at saturation. Following saturation of the high temperature peak, a second feature appeared at lower temperature with a broad peak at 910 K after large exposures. Based on previous studies of O_2 desorption following O_3 decomposition on Pt–Sn alloys [37], we can assign these two peaks to decomposition of Sn-oxide species. Our explanation of these two peaks is that the 1077-K peak is due to O_2 desorption from reduction of Sn–O–Sn species and the peak at 910 K is due to O_2 desorption from reduction of Sn–O–Pt species.

Fig. 4 utilizes the TPD areas from Figs. 1–3 to construct an uptake plot characterizing the adsorption kinetics and decomposition reactions during TPD. The NO_2 coverage scale was determined by calibration using the chemisorbed NO_2, NO, and O_2 TPD peak areas after NO_2 adsorption on clean Pt(1 1 1), assuming that 20% of the 0.5-ML NO_2 coverage desorbs as NO_2 and the rest decomposes cleanly to NO and O_2 during TPD as reported by Bartram et al. [5]. The NO and O_2 TPD areas in our experiments can be placed on this NO_2 coverage scale by assuming the sticking coefficient is constant, independent of coverage on the $\sqrt{3}$ alloy at 120 K, and noting that no other gas phase products were detected. The latter observation guarantees that NO:NO_2 is 1:1 and O_2: NO_2 is 1:2. Fig. 4 shows that the chemisorbed monolayer coverage is equivalent to 0.4-ML NO_2 and O_2 desorption at 1100 K represents an atomic oxygen coverage, θ_O, of 0.2 ML. Thus, oxygen associated with Sn sites on this surface, with $\Theta_{Sn} = 0.33$ ML, gives an O:Sn ratio of 2:3 corresponding to $Sn_{1.5}O$ species.

Fig. 5 demonstrates that the oxygen coverage can be increased by NO_2 exposures on the alloy at higher temperatures. The surface oxygen coverage obtained following exposures at 120 K is limited

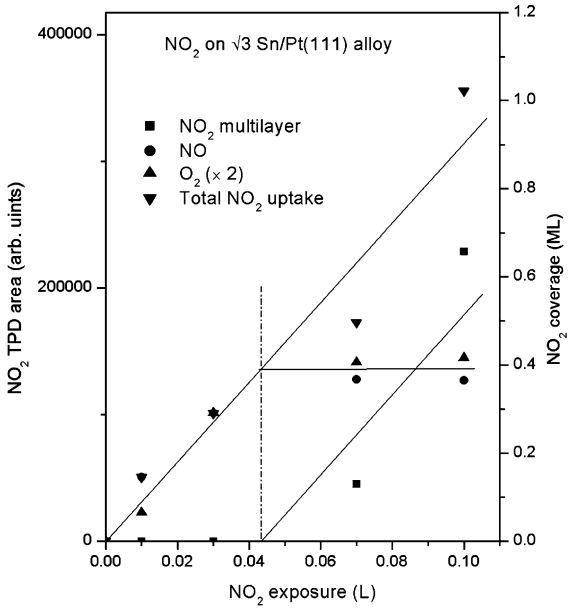

Fig. 4. Surface species concentrations as a function of NO_2 exposure to the $\sqrt{3}$ Sn/Pt(1 1 1) surface alloy at 120 K. The dashed vertical line indicates the NO_2 exposure that gives a surface with a saturation monolayer coverage.

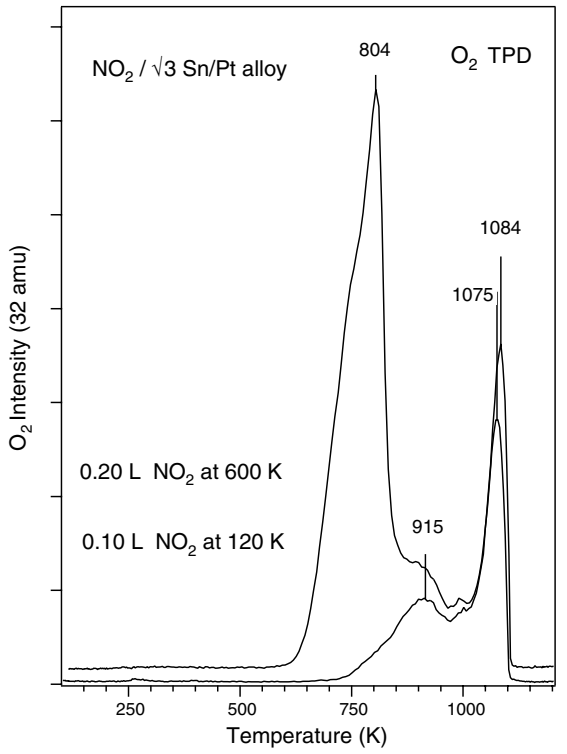

Fig. 5. O_2 desorption spectra resulting from NO_2 exposures on the $\sqrt{3}$ Sn/Pt(1 1 1) surface alloy: (top) 0.20 L NO_2 at 600 K; (bottom) 0.10 L NO_2 at 120 K.

by coadsorbed NO. The bottom curve in Fig. 5 reproduces the top curve from Fig. 3. The top curve in Fig. 5 is after a higher NO_2 exposure on the alloy at 600 K, which is above the desorption temperature of NO but below that required for O_2 desorption. This curve corresponds to $\theta_O = 1.1$ ML. This is a higher coverage than $\theta_O = 0.25$ ML obtained by O_2 exposure on Pt(1 1 1) at 150–300 K [38] and $\theta_O = 0.75$ ML obtained by NO_2 exposure on Pt(1 1 1) at 400 K [39]. This is also a higher coverage than reported by Saliba et al. [37] of $\theta_O = 0.87$ ML after O_3 exposures on the $\sqrt{3}$ alloy at 300 K. In that work, oxygen desorption below 850 K was associated with reduction of oxidic Pt species rather than SnO_x species. According to our results from Fig. 5, oxygen associated with Sn sites gives an O:Sn ratio of 0.5:0.33. This situation probably corresponds to forming $SnO_{1.5}$ species.

3.2. AES

The origin of the two O_2 desorption states seen in the TPD curves shown in Fig. 3 can be probed by chemical shifts in AES that are induced by reaction with adsorbates and indicate the oxidation state of the substrate components. The kinetic energies (KE) of emitted Auger electrons are affected by core level binding energy shifts and so they are useful for qualitatively assessing whether or not oxidation has occurred. Experiments utilizing this approach have been reviewed by Baker and Brundle [40].

Fig. 6 shows the shift in the Sn(MNN) AES peaks after exposures of 0.1-L NO_2 on the $\sqrt{3}$ alloy at 120 K and then subsequently heating the surface to gradually desorb O_2. On the $\sqrt{3}$ alloy, the lower KE Sn(MNN) peak is located at 426.6 eV, identical to the value for Sn metal [41]. After NO_2 exposure and annealing to 700 K, the peak shifts −1.5 to 425.1 eV KE. This indicates oxidation of Sn. However, this shift is much lower than that observed for bulk tin oxides surfaces, where

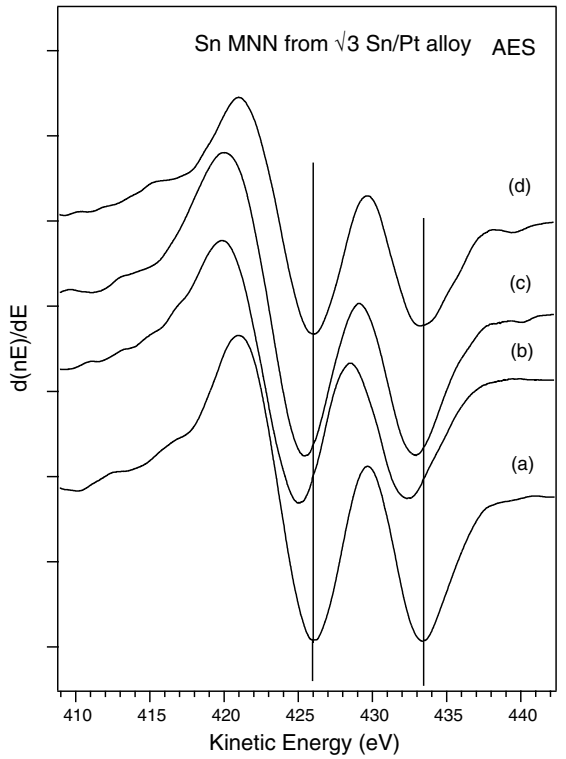

Fig. 6. Sn MNN Auger spectra of (a) clean $\sqrt{3}$ alloy (b) following 0.1 L NO_2 exposure to the $\sqrt{3}$ Sn/Pt(1 1 1) surface alloy at 120 and 700 K anneal (c) 900 K anneal and desorption of oxygen from Pt (d) 1220 K anneal and desorption of oxygen from Sn.

SnO (−3 to 423 eV) and SnO_2 (−7 to 419 eV) are characterized by large shifts when compared to metallic tin [41]. No such shift occurs at 120 or 200 K (not shown), demonstrating that Sn is not yet oxidized at those temperatures. The Sn(MNN) peak shifted to 425.4 eV KE following a 900 K anneal which caused some desorption of O_2. This shift can be explained by reduction of some oxidized Sn back to a metallic state in the alloy. The Sn peak returned to its original location at 426.6 eV KE after annealing to 1200 K, which removes all oxygen from the surface. Thus, Sn was completely reduced and the alloy reformed under these conditions. The 1200 K anneal also caused the intensity of the Sn peak to decrease and the LEED pattern to change to a superposition of (2×2) and $\sqrt{3}$ spots. Either desorption of Sn or diffusion of Sn into the bulk could account for this Sn reduction, which has been seen before [42]. This made it necessary to regenerate the $\sqrt{3}$ alloy after each NO_2 experiment by additional Sn dosing and annealing. No shift in the Pt(NOO) AES peak at 237 eV was ever observed during NO_2 adsorption at 120 K or after annealing. This is consistent with our assignment of the 804 K O_2 TPD peak in Fig. 5 to desorption of $O_{(a)}$ associated with Pt sites and the assignment of O_2 desorption above 850 K to decomposition of oxidized Sn species.

3.3. LEED

The $\sqrt{3}$ alloy was probed by LEED following a 0.1 L (~2 ML) dose of NO_2 on the sample at 120 K. This caused no change in the alloy LEED pattern other than to decrease the spot intensity, and no significant changes were observed after annealing to 200 K which desorbs some NO_2. After annealing to 280 K, which desorbs some NO, the spots from the $(\sqrt{3}\times\sqrt{3})R30°$ pattern disappeared and only the (1×1) spots of Pt(1 1 1) remained with a diffuse background. On some areas of the crystal, a faint (2×2) structure was observed, similar to that seen by Parker et al. [39] for $\theta_O = 0.25$ ML generated after NO_2 exposures on Pt(1 1 1). After a subsequent anneal to 700 K, (2×2) spots could no longer be seen and only a blurry (1×1) pattern remained. Annealing to 900 K desorbed all oxygen except that in the highest temperature O_2 TPD peak at 1020 K. This resulted in the appearance of a (4×4) LEED pattern, which is consistent with the observations of Batzill et al. [43]. In this condition, only oxygen remains at the surface and Sn is oxidized as shown in Fig. 6.

3.4. HREELS

Fig. 7 shows HREELS spectra following deposition of a multilayer film of NO_2 (~6 layers, $\theta_{NO_2} = 2.4$ ML) on the $\sqrt{3}$ alloy at 120 K and then subsequently heating the sample to increasing temperatures. The sample was heated to the indicated temperature for 30 s in each case and then re-cooled to 120 K and the spectra taken. Assignments of the energy loss peaks to specific vibrations are given in Table 1.

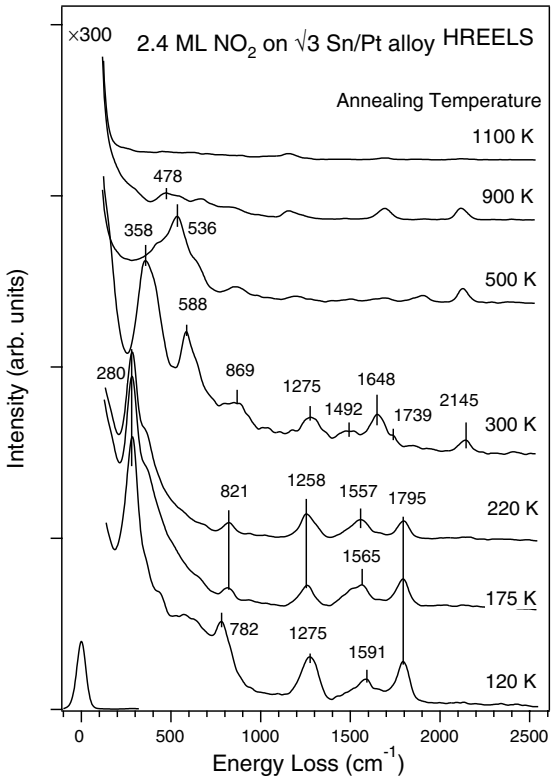

Fig. 7. HREELS warm-up experiments after 2.4 ML NO_2 adsorbed on the $\sqrt{3}$ Sn/Pt(1 1 1) alloy at 120 K. Reaction mechanism is shown on the right.

For the multilayer film at 120 K, loss peaks corresponding to the O–N–O symmetric (ν_{s,NO_2}) and asymmetric (ν_{as,NO_2}) stretching modes of the N,N-bonded dimer, N_2O_4, appear at 1275 and 1795 cm^{-1}, respectively. The N–N stretching mode (ν_{N-N}) of N_2O_4 occurs at 280 cm^{-1} and the O–N–O bending mode (δ_{NO_2}) of N_2O_4 appears at 782 cm^{-1}. A peak near the one at 1591 cm^{-1} has been assigned in the past [44] to a $2\delta_{NO_2}$ combination band, or more likely a double loss, in N_2O_4.

When the surface is annealed to 175 or 220 K, which desorbs any physisorbed multilayer species as shown in Fig. 1, surprisingly little change occurred in the HREELS spectra other than decreases in peak intensities consistent with some NO_2 desorption. This is a very different spectrum than that obtained for the μ-N,O-nitrito surface species, a chemisorbed NO_2 species bonded to the surface through both of the N and O atoms, formed on Pt(1 1 1) [5], the N-bonded chemisorbed NO_2 species formed on oxygen-precovered Pt(1 1 1) [45], and the O,O′-chelating surface species, a chemisorbed NO_2 species bonded to the surface through both of O atoms, formed on Au(1 1 1) [17]. Small peak shifts do occur upon desorption of the multilayer for the energy loss peaks at 782, 1275, and 1591 cm^{-1}. The close resemblence of the spectrum after heating to 220 K to that for the condensed film, especially the continued presence of the N–N stretch at 280 cm^{-1} identifies that the chemisorbed monolayer is comprised of N,N-bonded dimers of N_2O_4, characterized by vibrational modes at 280, 821, 1258, and 1795 cm^{-1}.

Table 1
Vibrational assignments for N_2O_4[a]

	Solid N_2O_4 [50]	N_2O_4 multilayer on Pt(1 1 1) [5]	N_2O_4 multilayer on $\sqrt{3}$ alloy (this work)	N_2O_4 monolayer on graphite [44]	N_2O_4 monolayer on O/Au(1 1 1) [45]	N_2O_4 monolayer on $\sqrt{3}$ alloy (this work)
$\nu O_2N–NO_2$ (stretch)	–	265	280	290	–	280
$\rho O_2N–NO_2$ (hindered rotation)	–	460	–	452	(440)	–
δNO_2 (bend)	737–752	795	782	782	750	821
$\nu_s NO_2$ (symmetric stretch)	1250	1290	1275	1290	1260	1258
$2\delta NO_2$ (combination band)	–	1540	1591	1557	–	1557
$\nu_a NO_2$ (asymmetric stretch)	1750	1770	1795	1758	1745	1795

[a] All data was obtained by HREELS except for solid N_2O_4 which was obtained by FTIR.

Table 1 provides results for other N_2O_4 monolayers identified on graphite [44] and oxygen-precovered Au(1 1 1) [45] surfaces. The close agreement between these spectra and ours support our assignment. The only small discrepancy has to do with the assignment of the loss peak at 1557 cm^{-1} for the monolayer; it would seem that this is better assigned to the ($\nu_{s,NO_2} + \nu_{N-N}$) combination band or double loss in N_2O_4. Furthermore, observation of an intense ν_{N-N} mode indicates that the N–N bond in N_2O_4 is oriented nearly along the surface normal, and certainly not near parallel with the surface plane, and observation of ν_{s,NO_2} and ν_{as,NO_2} modes in N_2O_4 with nearly the same intensity rules out both a flat-lying N_2O_4 with the molecular plane oriented parallel to the surface plane and an upright, chelating N_2O_4 species with C_{2v} symmetry oriented along the surface normal. We propose that the chemisorbed layer formed on the $\sqrt{3}$ alloy surface is an N,N-bonded dimer of N_2O_4 interacting with the surface through a single oxygen atom in an upright but tilted geometry.

Heating this chemisorbed layer to 300 K breaks the N–N bond and vibrations assigned to coadsorbed NO_2, NO and O are observed. The TPD spectra in Fig. 2 show that a large amount of NO desorption occurs by heating to 300 K, and consistently, only weak loss peaks due to the NO stretching mode in adsorbed NO was observed in the expected range of 1445–1718 cm^{-1} [36]. Vibrational losses observed at 1275 and near 869 cm^{-1} indicate that some molecularly adsorbed NO_2 remains on the surface. We assign this species to the N-bonded, chemisorbed NO_2 species with C_{2v} symmetry that is formed on oxygen-precovered Pt(1 1 1) [6]. However, in contrast to that case, the NO_2 adsorbed on the $\sqrt{3}$ Sn–Pt alloy surface fully decomposes at higher temperature with no evolution of gaseous NO_2. Other features of the spectrum include those due to a small amount of coadsorbed CO and H_2O contamination, and two large peaks at 358 and 588 cm^{-1}. We do not have a satisfactory explanation for the intensities of these latter two peaks, but metal–molecule stretching modes for NO_2 and NO, along with an NO bending mode for tilted NO species, can contribute losses in this region.

Annealing to 500 K removes all chemisorbed molecular species and only a broad feature centered at 536 cm^{-1} was observed. This feature is due to Sn–O vibrations that can occur over a wide range of energies depending on the structure and composition of the tin oxide film [46]. After heating to 900 K, which desorbs some oxygen from the surface, some small loss features due to Sn–O modes still remain, but these are eliminated by heating to 1100 K.

4. Discussion

4.1. Adsorption and bonding of NO_2

NO_2 adsorbs in the monolayer on the $(\sqrt{3} \times \sqrt{3})R30°$ Sn/Pt(1 1 1) surface alloy at 120 K as an upright N–N bonded, N_2O_4 dimer. This was determined by analysis of the specular vibrational spectrum obtained by HREELS. The surface dipole selection rule requires an adsorption geometry that has the molecular plane tilted with respect to the surface normal for observation of the asymmetric (ν_{as,NO_2}) stretching mode of N_2O_4 at 1795 cm^{-1}, and we propose a monodentate O-bonded species. NO_2 dimerization has been observed to produce an N_2O_4 species in the monolayer on graphite at 90 K [44] and bound to the oxygen-precovered Au(1 1 1) surface at 86 K [45]. N_2O_4 in the chemisorbed monolayer is not typically formed from NO_2 exposures on Group-VIII transition metal surfaces even at temperatures of 85–100 K, because the N–N bond energy is only 13 kcal/mol [47] and strong chemisorption of two individual NO_2 molecules is preferred. Alloying Sn into the Pt(1 1 1) surface reduces the surface reactivity such that the strongly chemisorbed μ-N,O-bonded-nitrito species of NO_2 on Pt(1 1 1) is not formed on the alloy. Rather, as on the relatively chemically inert gold and graphite surfaces, the N–N bonded dimer of N_2O_4 is formed on the $\sqrt{3}$ alloy at 120 K. However, presumably this is a kinetic problem due to an activation energy barrier that must be surmounted prior to formation of strongly chemisorbed NO_2. Evidence for this conclusion is that we observed with HREELS a chemisorbed N-bonded, molecular NO_2 species in

the monolayer formed after heating and this species reacted irreversibly at higher temperatures. Also, NO_2 exposures carried out on the $\sqrt{3}$ alloy at 600 K led to extensive NO_2 decomposition and oxidation of the surface.

4.2. Surface oxidation

Decomposition of NO_2 occurs on the $\sqrt{3}$ alloy between 220 and 300 K to liberate surface oxygen and coadsorbed NO. Surface oxygen oxidizes Sn in the $\sqrt{3}$ alloy at higher temperatures. The evidence presented herein for that was the Sn–O vibrations seen in HREELS after heating to 500 K and −1.5-eV shift in the Sn(MNN) AES transition after heating to 700 K. O_2 desorption from Sn sites occurs at higher temperatures than from Pt sites. This is in agreement with a higher Sn–O bond strength, which is expected from the known heats of formation (ΔH_f^0) of tin oxide (SnO, −68.3 kcal/mol; SnO_2, −138.8 kcal/mol) compared with platinum oxide (PtO_2, +41.0 kcal/mol; Pt_3O_4, −39 kcal/mol) [48].

Batzill et al. [46] found by using XPS three Sn ($3d_{5/2}$) peaks at 484.6, 485.0, and 486.0 eV following oxidation by NO_2 of the $\sqrt{3}$ alloy at 400 K. These XPS peaks were assigned as due to metallic, "quasimetallic", and Sn^{4+} species, respectively, with the largest fraction of Sn present in the "quasimetallic" state. This chemical state was recently assigned to oxidized Sn that is still alloyed (strongly bonded) with Pt in the surface layer [43].

We find that after desorption of all surface-bound NO and oxygen associated with Pt sites, $\theta_O = 0.2$ ML remains at the surface associated with oxidized Sn species. With $\Theta_{Sn} = 0.33$ ML, this gives an O:Sn ratio of 2:3 corresponding to surface film of $Sn_{1.5}O$ species. This condition also produces a (4×4) LEED pattern. Other more detailed STM and LEED studies of oxidation of the $\sqrt{3}$ alloy by using NO_2 are reported elsewhere [43], but our LEED observations agree with theirs when the $\sqrt{3}$ alloy was oxidized at the same temperature. Annealing to 900–1000 K, or annealing to 850 K for several minutes, caused formation of the (4×4) pattern. The model developed from the STM images for the (4×4) structure proposed that Sn_xO_y "pseudomolecules" formed ordered chains along high symmetry directions on a (2×2)Sn/Pt(1 1 1) surface alloy. Oxygen atoms are bonded to both Sn adatoms in the chains and alloyed Sn in the surface layer. They estimated that the stoichiometry of this layer was SnO but allowed for an upper limit of Sn_2O. Our determination that $Sn_{1.5}O$ species correspond to this structure is consistent with either proposal.

Our results following NO_2 exposures on the alloy at 600 K is also consistent with previous structural models developed for more heavily oxidized alloys [43]. In our work, oxygen associated with Sn sites after more extensive oxidation reactions corresponds to forming $SnO_{1.5}$ species. This confirms the previous report that a complete SnO_2 film cannot be formed abruptly at the Pt substrate interface, but rather a reduced SnO_x interfacial layer (or layers) is required.

Previous results using XPS conclude that Pt is not oxidized by reactions of NO_2 on the $\sqrt{3}$ alloy under UHV conditions such as those investigated in this report [46]. We did not observe any shift of the Pt AES peak at 237 eV upon adsorption or reaction of NO_2, and so we would agree with that conclusion. Consistent with expectations, NO_2 is a weaker oxidant than ozone (O_3). Saliba et al. [49] observed a Pt AES shift of −0.8 eV after the adsorption of 2 ML of oxygen atoms using ozone (O_3) exposures on Pt(1 1 1) at 300 K and attributed this, along with a sharp, intense peak near 800 K in subsequent O_2 TPD spectra, to Pt oxidation. By contrast, Parker et al. [39] noted no Pt AES shift for the adsorption of up to 0.75 ML of oxygen adatoms and no sharp O_2 TPD peak resulting from NO_2 exposures on Pt(1 1 1). O_3 adsorption also leads to Pt oxidation on either of the (2×2) or $\sqrt{3}$ Sn/Pt(1 1 1) alloys based on the appearance of the O_2 TPD spectra [37].

5. Conclusion

NO_2 exposures to produce a saturation monolayer coverage on a $(\sqrt{3} \times \sqrt{3})R30°$ Sn/Pt(1 1 1) surface alloy at 120 K form an N–N bonded dimer, N_2O_4, adsorbed in an upright, tilted geometry. We propose that this is a monodentate species, bonding through a single oxygen atom to the surface.

No N_2O_4 or NO_2 desorbs molecularly from the chemisorbed monolayer. The dimer completely dissociates between 220 and 300 K, leaving coadsorbed NO_2, NO, and O at the surface. Chemisorbed NO_2 in this adlayer is present as a N-bonded nitrite species bound to the surface via the nitrogen atom. This species is irreversibly adsorbed and decomposes completely during further heating.

NO_2 decomposition leads to surface oxygen and oxidation of Sn in the $\sqrt{3}$ alloy at higher temperatures. Pt is not oxidized under these conditions. The maximum oxygen coverage obtained by heating the N_2O_4 monolayer was $\theta_O = 0.4$ ML. Heating to 900 K leaves $\theta_O = 0.2$ ML at the surface associated with oxidized Sn species, corresponding to an ordered surface film of $Sn_{1.5}O$ species exhibiting a (4×4) LEED pattern. Oxidation of the alloy can be increased by dosing NO_2 on the surface held at 600 K, which keeps the surface free of coadsorbed NO and provides thermal energy for activated NO_2 dissociation. In this case, an oxygen coverage of $\theta_O = 1.1$ ML can be initially obtained. Heating this surface to 900 K produces a film with a stoichiometry of $SnO_{1.5}$, and not a fully oxidized SnO_2 layer.

Oxygen is liberated from reduction of the alloy in three O_2 thermal desorption peaks: two higher temperature peaks at 915 and 1084 K due to the decomposition of oxidized Sn species; and a lower temperature peak at 804 K due to chemisorbed O adatoms associated with Pt sites.

Acknowledgements

This work was funded partially by the Army Research Office and the Division of Chemical Sciences, Office of Basic Energy Sciences, US Department of Energy. We thank Drs. Harald Busse and Hong He for their assistance with experiments. Also, we thank Drs. Najat Saliba and Jiang Wang for helpful discussions.

References

[1] M.A. Hitchman, G.L. Rowbottom, Coordination Chem. Rev. 42 (1982) 55.
[2] K.C. Taylor, in: J.R. Anderson, M. Boudart (Eds.), Catalysis Science and Technology, vol. 5, Springer, Berlin, 1984, p. 119.
[3] D.W. Fahey, C.S. Eubank, G. Hubler, F.C. Fehsenfeld, J. Atmos. Chem. 3 (1985) 435.
[4] S.A. Nyarady, R.E. Sievers, J. Am. Chem. Soc. 107 (1985) 3726.
[5] M.E. Bartram, R.G. Windham, B.E. Koel, Surf. Sci. 184 (1987) 57.
[6] M.E. Bartram, R.G. Windham, B.E. Koel, Langmuir 4 (1988) 240.
[7] U. Schwalke, J.E. Parmeter, W.H. Weinberg, J. Chem. Phys. 84 (1986) 4036.
[8] U. Schwalke, J.E. Parmeter, W.H. Weinberg, Surf. Sci. 178 (1986) 625.
[9] D.A. Outka, R.J. Madix, G.B. Fisher, C. Dimmagio, Surf. Sci. 179 (1987) 1.
[10] S.R. Bare, K. Griffiths, W.N. Lennard, H.T. Tang, Surf. Sci. 342 (1995) 185.
[11] G. Polzonetti, P. Alnot, C.R. Brundle, Surf. Sci. 238 (1990) 226.
[12] G. Polzonetti, P. Alnot, C.R. Brundle, Surf. Sci. 238 (1990) 237.
[13] W.A. Brown, P. Gardner, D.A. King, Surf. Sci. 330 (1995) 41.
[14] D.I. Wickham, B.A. Banse, B.E. Koel, Surf. Sci. 243 (1991) 83.
[15] M.E. Bartram, B.E. Koel, Surf. Sci. 213 (1989) 137.
[16] J. Wang, M.R. Voss, H. Busse, B.E. Koel, J. Phys. Chem. B 102 (1998) 4693.
[17] J. Wang, B.E. Koel, J. Phys. Chem. A 102 (1998) 8573.
[18] M. Beckendorf, U.J. Katter, H. Schlienz, H.J. Freund, J. Phys. C 5 (1993) 5471.
[19] B.H. Davis, in: M.E. Davis, S.L. Suib (Eds.), Selectivity in Catalysis, vol. 517, American Chemical Society, Washington, 1993, p. 109.
[20] M.T. Paffett, S.C. Gebhard, R.G. Windham, B.E. Koel, Surf. Sci. 223 (1989) 449.
[21] C. Xu, J.W. Peck, B.E. Koel, J. Am. Chem. Soc. 115 (1993) 751.
[22] C. Xu, B.E. Koel, Surf. Sci. 304 (1994) 249.
[23] C. Xu, Y.L. Tsai, B.E. Koel, J. Phys. Chem. 98 (1994) 585.
[24] C. Xu, B.E. Koel, M.T. Paffett, Langmuir 10 (1994) 166.
[25] J.W. Peck, B.E. Koel, J. Am. Chem. Soc. 118 (1996) 2708.
[26] Y.L. Tsai, C. Xu, B.E. Koel, Surf. Sci. 385 (1997) 37.
[27] H. Lieske, J. Völter, J. Catal. 90 (1984) 96.
[28] E. Merlen, P. Beccat, J.C. Bertolini, P. Delichère, N. Zanier, B. Didillon, J. Catal. 159 (1996) 178.
[29] K. Grass, H.G. Lintz, J. Catal. 172 (1997) 446.
[30] L. Promsong, M. Sriyudthsak, Sensor. Actuat. B 24–25 (1995) 504.
[31] P.P. Tsai, I.C. Chen, M.H. Tzeng, Sensor. Actuat. B 24–25 (1995) 537.
[32] M.T. Paffett, S.C. Gebhard, R.G. Windham, B.E. Koel, J. Phys. Chem. 94 (1990) 6831.
[33] H. Zhao, J. Kim, B.E. Koel, Surf. Sci. 538 (2003) 147.

[34] Y.D. Li, M.R. Voss, N. Swami, Y.L. Tsai, B.E. Koel, Phys. Rev. B 56 (1997) 15982.
[35] C.T. Campbell, S.M. Valone, J. Vac. Sci. Technol. A 3 (1985) 408.
[36] C. Xu, B.E. Koel, Surf. Sci. 310 (1994) 198.
[37] N.A. Saliba, Y.L. Tsai, B.E. Koel, J. Phys. Chem. B 103 (1999) 1532.
[38] C. Puglia, A. Nilsson, B. Hernnäs, O. Karis, P. Bennich, N. Mårtensson, Surf. Sci. 342 (1995) 119.
[39] D.H. Parker, M.E. Bartram, B.E. Koel, Surf. Sci. 217 (1989) 489.
[40] A.D. Baker, C.R. Brundle, in: C.R. Brundle, A.D. Baker (Eds.), Electron Spectroscopy: Theory, Techniques, and Applications, vol. I, Academic Press, New York, 1977, p. 1.
[41] S.K. Sen, S. Sen, C.L. Bauer, Thin Solid Films 82 (1981) 157.
[42] M.T. Paffett, R.G. Windham, Surf. Sci. 208 (1989) 34.
[43] M. Batzill, D.E. Beck, B.E. Koel, Phys. Rev. B 64 (2001) 245402.
[44] P. Sjövall, S.K. So, B. Kasemo, R. Franchy, W. Ho, Chem. Phys. Lett. 172 (1990) 125.
[45] J. Wang, M.E. Bartram, B.E. Koel, in press.
[46] M. Batzill, J. Kim, D.E. Beck, B.E. Koel, Phys. Rev. B, submitted for publication.
[47] J.A. Kerr, Ann. Rep. Chem. Soc. A 64 (1967) 73.
[48] R.C. Weast, CRC Press, Inc., Boca Raton, 1989, vol. 70.
[49] N.A. Saliba, Y.L. Tsai, C. Panja, B.E. Koel, Surf. Sci. 419 (1999) 79.
[50] A. Givan, A. Loewenschuss, J. Chem. Phys. 93 (1990) 866.